

Effects of optical attenuation, heat diffusion and acoustic coherence in photoacoustic signals produced by nanoparticles

J. E. Alba-Rosales,¹ G. Ramos-Ortiz,² L. F. Escamilla-Herrera,³ B. Reyes-Ramírez,² L. Polo-Parada,^{4, a)} and G. Gutiérrez-Juárez^{1, b)}

¹⁾*División de Ciencias e Ingenierías, Universidad de Guanajuato. León, Gto., México.*

²⁾*Centro de Investigaciones en Óptica. León, Gto., México.*

³⁾*Instituto de Ciencias Nucleares, UNAM, CDMX, México.*

⁴⁾*Dalton Cardiovascular Research Center, Department of Medical Pharmacology and Physiology, University of Missouri-Columbia, Columbia, MO, USA.*

(Dated: 4 February 2022)

Behavior of the photoacoustic signal produced by nanoparticles as a function of their concentration was studied in detail. As the concentration of nanoparticles is increased in a sample, the peak-to-peak photoacoustic amplitude increases linearly up to a certain value, after which an asymptotic saturated behavior is observed. To elucidate the mechanisms responsible for these observations, we evaluate the effects of nanoparticles concentration, the optical attenuation and the effects of heat propagation from nano-sources to their surroundings. We found that the saturation effect of the photoacoustic signal as a function the concentration of nanoparticles is explained by a combination of two different mechanisms. As has been suggested previously, but not modeled correctly, the most important mechanism is attributed to optical attenuation. The second mechanism is due to an interference destructive process attributed to the superimposition of the photoacoustic amplitudes generated for each nanoparticle, this explanation is reinforced through our experimental and simulations results; based on this, it is found that the linear behavior of the photoacoustic amplitude could be restricted to optical densities ≤ 0.5 .

PACS numbers: 78.20.Hp

Keywords: Photoacoustics, Nanoparticles, Interference, Saturation

In recent years, pulsed laser-induced ultrasound (US), better known as the Photoacoustic (PA) effect, has had a major resurgence because its wide range of applications, mainly in the biological and medical areas¹, for instance, PA imaging² and as monitoring method in thermo-therapy of cancer³. Further the analogies between optical and acoustic phenomena, led to advancements in confocal PA microscopy⁴, creations of new methodologies to detect US⁵ and generation of new materials to achieve thermal and/or acoustic contrasts⁶. PA effect is produced by the absorption of CW modulated pulsed optical radiation by a medium. This absorption raises non-radiative decays that increase the temperature and causes mechanical waves typically in the range of US. The major advantages for PA techniques are their sensibility to distinguish different optical contrast and the US penetration in the tissue⁷.

Nowadays metallic nanoparticles (NPs) play an important role as enhancers of the PA signal, the design and application of these materials is subject to the type of applications desired, as well as to the available laser source.^{1,8,9}

Previous reports have shown that the PA amplitude is not always proportional to materials concentration; for example, the first reports of PA saturation are de-

scribed in the work of J. W. Pin¹⁰ and J. Wang¹¹; in the later, authors employ a continuous absorption model to explain the saturation in red ink, but such model depends of multiple parameters (without physical meaning) adjustment to correctly fit the experimental data. Notwithstanding this deficiency, this reference has been the explanation for the PA saturation obtained in dyes, pigments and tissue. On the other hand, despite the different physical properties exhibit by NPs, a similar saturation effect is observed. In several cases a linear dependence between amplitude and concentration has been obtained; for example, gold (Au) nano-vesicles³, Au nano-rods⁹, Au bio-conjugated nano-spheres^{12,13}, silica-coated Au nano-rods¹⁴, Au nano-carbon-tubes and Fe₂O₃ nano-spheres¹⁵; while, in many other examples a saturated behavior is observed; Au nano-spheres¹⁶, Au nano-cages¹⁷ and Au nano-beacons¹⁸. The origin of this discrepancy has been never analyzed in detail and there are few reports where the PA response from a discretized system in micro scale was obtained¹⁹⁻²¹.

Also, the PA signal shape at low concentrations has been observed that is symmetric whereas at high concentrations became asymmetric; this behavior has been extensively reported in the literature^{4,13,19,21-28}. Therefore, the goal of this study is to explain the causes of these concentration-dependent effects. Herein it is proposed that the key characteristics of the nonlinear saturated behavior in the peak-to-peak (P-P) PA amplitude and its asymmetry at high concentrations are explained

^{a)}Electronic mail: poloparadal@missouri.edu

^{b)}Electronic mail: ggutj@fisica.ugto.mx

by means of a photo-thermo-acoustic model²⁹. Sigrist²² previously reported a model that explained the PA signal produced by a continuous media (liquids); in this paper, the model is extended to a discrete case from continuous media to NPs. The NPs are represented by single point that absorbs the incident radiation instantaneously³⁰. With this model a simulation code was developed taking in account the heat source size, the light attenuated by the NPs and the coherence of a single PA signal source^{29,31}. The light losses, by absorption and scattering, can be described by the well-known Beer-Lambert (BL) law, which corresponds to an exponential decay in the amount of light. We hypothesize that the asymmetric shape of the PA signals is due to the interference of the individual PA signals generated by the NPs. To verify this, it is theoretically estimated the spatial region where interference of two PA waves occurs. These results are of great importance in applications where the NPs are used as a PA enhancer, since they allow to identify a dynamic range for PA amplitude generation and an optimal contrast agent concentration at which the maximum PA signal contrast is possible.

For this, PA experiments were conducted with 5, 10 and 100 nm Au NPs (spheres, nanoComposix) in 2 mM sodium citrate dihydrate aqueous solution (Detailed information about the samples characteristics can be found in supplementary information). The suspensions optical density (OD)^{32,33} were measured as a function of the NPs concentration for each aliquot by using an UV-VIS spectrometer (Lambda 900 UV/VIS/NIR, Pekin Elmer). The experimental setup for the detection of PA signals is shown in Figure 1. The second harmonic from a Nd:YAG pulsed laser (Brilliant, Quantel) was employed to provide 532 nm light with a pulse duration of 10 ns and a repetition rate of 10 Hz. This beam was focused into the PA cell using a couple of lenses such that a large Rayleigh waits length was obtained to be approximately constant inside the cell (0.7 mm of diameter). The energy per pulse was set at 1 mJ ($\pm 5\%$, SD). The laser beam was set perpendicular to the transducer 2 mm away. The laser energy was monitored using a thermopile (1917-R, Newport) coupled to a power meter (818P-030-19, Newport). PA signals were detected with a homemade transducer (20 MHz central response and a bandwidth of 20 MHz)³⁴ and displayed by a 200-MHz oscilloscope (TDS5104B, Tektronix, Wilsonville, OR) triggered by a photo-diode (DET10A; Thorlabs, Newton, NJ) with a 1-nanoseconds rise time. The signals were amplified with a gain of 25 dB via 500 MHz amplifier (ZFL-500LN-BNC+, Mini-Circuits). NPs suspensions were diluted from stock concentration (100%) in steps of 10% using a sodium citrate aqueous solution at 2 M (6028, Karal).

Figure 2(a) shows the PA signals generated by the NPs suspensions at stock concentration, these are 4×10^{13} for 5 nm, 5×10^{12} for 10 nm and 5×10^9 for 100 nm. The signals generated by the NPs are observed at 1.3 μ s. For lower NPs concentrations, the PA signals exhibited similar shape, but smaller amplitudes. Figures 2 (b) to

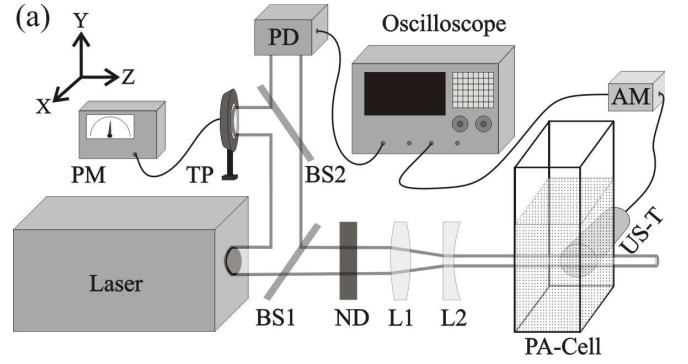


FIG. 1. Experimental setup. PD: photo-diode, AM: amplifier, PM: power meter, TP: thermopile, ND: neutral density filters, BS1: beam splitter 10:90, BS2: beam splitter 10:90, L1: plane-convex lens with $f = +300$ mm, L2: plane-concave lens with $f = -50$ mm, US-T: ultra sound transducer. The distance between L1 and L2 is 250 mm.

2 (d) show the respective normalized P-P PA amplitudes as a function of the NPs concentration for each NP size.

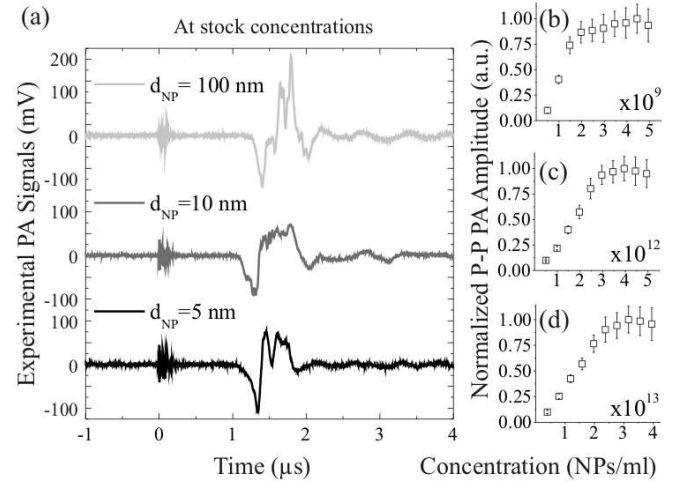


FIG. 2. (a) Measured PA signals obtained from different NPs samples at stock concentration. (b)-(d) Normalized PA amplitude as a function of concentration for each NPs of 100 nm, 10 nm and 5 nm, respectively.

Here, it is assumed that the measured pressure $p(\mathbf{R}, t)$ in \mathbf{r} generated by a single nanoparticle (NP) at \mathbf{r}' is described by^{22,30,35,36}:

$$p(\mathbf{R}, t) = p_0 \frac{ct - |\mathbf{R}|}{|\mathbf{R}|} \exp \left[- \left(\frac{ct - |\mathbf{R}|}{d_0/2} \right)^2 \right]; \quad (1)$$

with $p_0 = 4E_0\beta c^2/\pi^{3/2}C_p d_0^3$ and $\mathbf{R} = \mathbf{r} - \mathbf{r}'$. Here E_0 β , c , and C_p , are the the energy per pulse, the thermal expansion coefficient, the sound speed medium propagation and the heat capacity at constant pressure of the

fluid sample, respectively. In Sigrist paper, d_0 was defined as the spatial illumination profile of a Gaussian beam²². However, we associate this parameter with the thermal size of the object. This hypothesis is justified from the assumption that a NP only can absorb radiation, due to plasmonic effect⁸, meanwhile the surrounding fluid medium (water) does not. According to this, a minimum value for d_0 is the NP diameter (d_{NP}); and as maximum the quantity ($d_{NP} + d_{th}$) where:

$$d_{th} = 4(\chi_w \tau_l)^{\frac{1}{2}}. \quad (2)$$

Equation (2) is related the thermal diffusion length³⁷; for this expression χ_w is the water diffusivity ($0.143 \times 10^6 \text{m}^2/\text{s}$) and τ_l is the laser pulse (FWHM of 10 ns); therefore, $d_{th} = 150$ nm. This analytical approximation is equivalent to solve the coupling heat and pressure equations considering the laser time profile.

A code was written in the software Wolfram MathematicaTM to emulate the experiments performed. Considering the equation (1) and the optical attenuation, the numerical expression employed was:

$$p_{sim}(\mathbf{D}_{ij}, t) = \sum_{i=1, j=1}^{n, m} 10^{-\epsilon \zeta j \Delta z} \times p(\mathbf{D}_{ij}, t); \quad (3)$$

with $\mathbf{D}_{ij} = \mathbf{s} - \mathbf{r}_{ij}$. Here ϵ corresponds to the extinction coefficient and ζ is the sample concentration, which were measured for each NPs aliquot by UV-VIS spectroscopy. Likewise, \mathbf{s} corresponds to the sensor position. Counters i and j are used to label each NP and the cylinder section, respectively, the length of the sections is Δz . The complete methodology details used to perform the simulations can be found in the supplemental material.

In Figures 3a to 3c simulated PA signals for stock concentration and $d_0 = d_{NP}$ are presented. A statistical study shows that all signals are symmetric with well defined maximum and minimum peaks, which always appear near the center temporal range. To obtain the P-P PA amplitude it was sought the higher and lower peaks values for each individual simulation. Same behavior was observed when the BL law is considered, nonetheless, the maximum amplitude is diminished, as expected, being 60% less when compared to the case without attenuation.

In Figures 3d-3f, a comparison between the experimental and simulated P-P PA amplitudes as a function of the NPs concentration is shown; all data were normalized to the respective maximum amplitude. Simulations for $d_0 = d_{NP}$ without BL law predict completely the experimental trend, but when the optical attenuation is considered it fails; contrary to the expected results, the inclusion of BL law in the model did not predict the experiments. Trying to understand this discrepancy, the numerical Fourier transform can be performed to the simulated signals, when doing this a broad spectra are predicted with high central frequencies for $d_0 = d_{NP}$. The frequencies are at 100 GHz for the 5 nm and 10 nm samples and at 10 GHz for 100 nm; however, this is not in

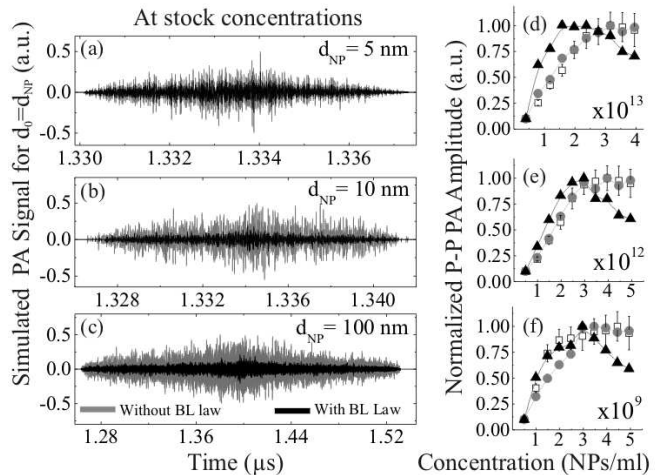


FIG. 3. (a)-(c) Simulated PA signals for $d_0 = d_{NP}$ at stock concentration for NPs of 5 nm, 10 nm and 100 nm respectively; the gray lines are the simulations without BL law and the black ones with BL. (d)-(f) Corresponding comparison between simulated and experimental P-P PA amplitudes as a function of concentration, squares for experimental data, circles for simulations without BL law and triangles for simulations with BL law. All data is normalized.

agreement with the actual spectral response of the sensors that we used in our experiments, then the $d_0 = d_{NP}$ assumption must be discarded.

In Figures 4a to 4c, simulations supposing $d_0 = d_{NP} + d_{th}$ are shown for the stock concentration of NPs. There are two aspects that must be highlighted: First, amplitude-shape for 5 and 10 nm samples are well-defined for all simulated concentrations; however, for 100 nm NPs it remains noisy, but its shape is more defined than for the case $d_0 = d_{NP}$. Second, opposite to the above case, PA signals are asymmetric for all samples, being like the experimental results and the reported literature. Considering BL law still decreases the PA amplitude approximately at 40% of the non-attenuated value. Comparison between experimental and simulated P-P PA amplitudes as a function of the NPs concentration is presented in Figures 4d to 4f. The simulated PA signals without BL law are linear. When light attenuation is considered, behavior of experimental signals is well predicted; as in the previous cases, the spectra for the simulated signals can be calculated numerically, the obtained frequencies now are between 1 and 100 MHz. For both sets of simulations, optical attenuation, through BL law, defines the amplitude of pressure wave and its effect is only to decrease the total PA amplitude.

To better understand the consequences for choosing a d_0 value, three aspects must be considered. First, from the PA power spectrum of a single NP it is found that the maximum frequency value occurs at $\nu_{max} = c/\sqrt{2\pi}(d_0/2)$. From this value can be calculated the spatial region where pulse of one NP can interact with each other, it corresponds to $\lambda \equiv \sqrt{2\pi}d_0$. Second, from the

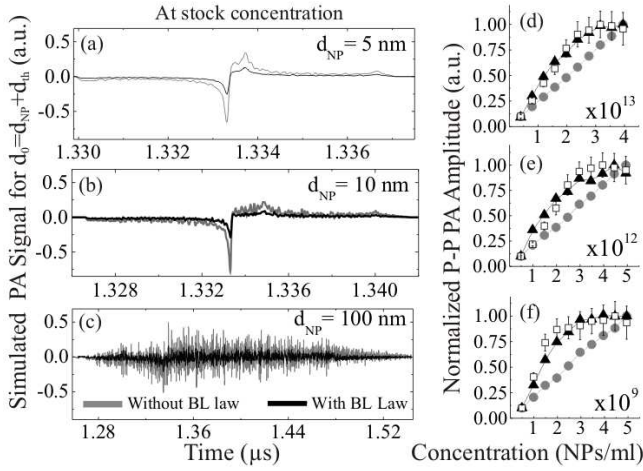


FIG. 4. (a)-(c) Simulated PA signals for $d_0 = d_{NP} + d_{th}$ at stock concentration for NPs of 5 nm, 10 nm and 100 nm respectively; the gray lines are the simulations without BL law and the black ones with BL. (d)-(f) Corresponding comparison between simulated and experimental P-P PA amplitudes as a function of concentration, squares for experimental data, circles for simulations without BL law and triangles for simulations with BL law. All data is normalized.

specific volume of the NPs suspension, an average distance between NPs L , can be determined. Third, equation (1) is proportional to the time derivative of a Gaussian function, which has a bipolar temporal profile i.e., it is composed of a compression and rarefaction cycle. When summation over two individual PA signals is performed at the measuring point, there are three extreme possible situations for the time delay (or acoustical path difference Δl), namely: (i) it is equal to zero, then the PA pulses match exactly and only constructive interference appears. (ii) it is equal to $\lambda/2c$; then, the rarefaction of one pulse corresponds exactly to the compression of another pulse, and therefore partial destructive interference is produced. (iii) It is greater than λ/c , so they cannot superimpose. These cases are displayed in Figures 5a to 5c. Using the above information, the ratios L/λ where calculated for all d_0 values and are shown in Figure 5d. When $d_0 = d_{NP}$, $L/\lambda \gg 1$ for all NP diameters and all NP concentrations, thus a high number of NPs cannot be superimposed; therefore, the sum of the individual signals, at the measurement point during a time interval, looks noisy and symmetric. For $d_0 = d_{NP} + d_{th}$, we can see in Figure 5d that $L/\lambda < 2$ for $d_{NP} = 5$ nm and $d_{NP} = 10$ nm, respectively; now summation over individual signals produces well defined shape and asymmetric PA signals with linear behavior of the P-P PA amplitudes as a function of the NPs number. This is because at the measurement point, in the time interval, the superposition of individual pressure waves occurs. For $d_0 = 100$ nm + d_{th} the corresponding ratio is in the range $5 < L/\lambda < 12.5$, then the interference is more probable than the case $d_0 = 100$ nm, but less when $d_0 = d_{NP} + d_{th}$ for 5 nm and 10 nm. The consequence for adding individ-

uals PA pulses, considering the heat diffusion from the NP volume to their surroundings, gives a PA signal with high signal-to-noise ratio, asymmetric shape peaks and a linear behavior in the P-P PA amplitude as a function of the NPs number. When the optical attenuation is taken into account the simulated PA amplitudes lose their linear dependence with the NPs concentration and the signal saturates, predicting properly the experimental results.

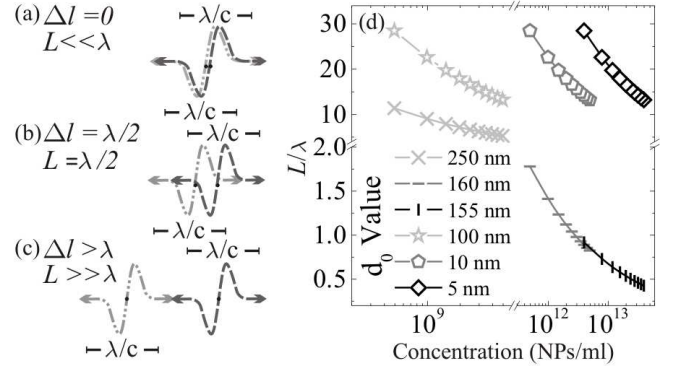


FIG. 5. (a)-(c) Present the three extreme possible configurations between the sources, totally constructive interference, partial destructive interference and when the signals can be superposed, respectively. (d) Ratios L/λ , for all d_0 values used in the simulations.

It is important to remark that, if the results are displayed as a function of the NPs OD instead of their concentrations, the nonlinear behavior of the P-P PA amplitudes is given for $OD \geq 0.5$. A meticulous review of the references^{3,9,11-21} is in concordance with this threshold (see supplementary data).

In summary, when heat propagates beyond the individual NPs volume and the optical attenuation of the sample is ignored, the P-P PA amplitude as a function of NPs concentration is linear; this extended PA source can improve the interference between the single US pulses. The simulations showed that asymmetric shape of the PA signal is obtained under this condition. When the heat is confined inside the NP dimensions, symmetric signals are obtained and a nonlinear P-P PA amplitude; the NP thermal confinement can be discarded through frequency spectrum too. The saturated behavior of P-P PA amplitude for the extended thermal source is correctly explained when the optical attenuation is considered. Finally, our simulations and experimental results showed that no linear behavior appears for an $OD \geq 0.5$. This threshold was well-matched with previous experimental reports. This value can be taken as a point of departure to obtain linear PA amplitudes as a function of the concentration for NPs samples.

Acknowledgments. The computation for this work was performed on the high-performance computing infrastructure provided by Research Computing Support Services and in part by the National Science Foundation under grant number CNS-1429294 at the University of Missouri, Columbia Mo. The experimental part of this

work was financed with the 2nd edition of UG-CIO research grants and CONACyT (grant number 5215708). Authors thank to Martin Olmos and Enrique Noe Arias for their support in this research and CONACyT.

- ¹W. Li and X. Chen, "Gold nanoparticles for photoacoustic imaging," *Nanomedicine* **10**(2), 299–320 (2015).
- ²T. Chaigne, J. Gateau, M. Allain, O. Katz, S. Gigan, A. Sentenac, and E. Bossy, "Super-resolution photoacoustic fluctuation imaging with multiple speckle illumination," *Optica* **3**, 54–57 (2016).
- ³P. Huang and *et al.*, "Biodegradable gold nanovesicles with an ultrastrong plasmonic coupling effect for photoacoustic imaging and photothermal therapy," *Angewandte Chemie International Edition* **52**, 13958–13964 (2013).
- ⁴L. Wang, C. Zhang, and L. V. Wang, "Grüneisen relaxation photoacoustic microscopy," *Phys. Rev. Lett.* **113**, 174301 (2014).
- ⁵C. Chao, S. Ashkenazi, S. Huang, M. O'Donnell, and L. Guo, "High-frequency ultrasound sensors using polymer microring resonators," *IEEE Transactions on Ultrasonics, Ferroelectrics, and Frequency Control* **54**, 957–964 (2007).
- ⁶F. Gao, X. Feng, and Y. Zheng, "Advanced photoacoustic and thermoacoustic sensing and imaging beyond pulsed absorption contrast," *Journal of Optics* **18**, 074006 (2016).
- ⁷L. Wang, *Photoacoustic Imaging and Spectroscopy* (CRC Press, Taylor & Francis Group, UK, 2009) p. xiii.
- ⁸T. H. D. M. W. Yujun Zhong, Shyamala Devi Malagari, "Review of mid-infrared plasmonic materials," *Journal of Nanophotonics* **9**, 9–9–21 (2015).
- ⁹C. L. Bayer, S. Y. Nam, Y.-S. Chen, and S. Y. Emelianov, "Photoacoustic signal amplification through plasmonic nanoparticle aggregation," *Journal of Biomedical Optics* **18**, 16001 (2013).
- ¹⁰J. W. Lin and L. P. Dudek, "Signal saturation effect and analytical techniques in photoacoustic spectroscopy of solids," *Analytical Chemistry* **51**, 1627–1632 (1979).
- ¹¹J. Wang, T. Liu, S. Jiao, R. Chen, Q. Zhou, K. K. Shung, L. V. Wang, and H. F. Zhang, "Saturation effect in functional photoacoustic imaging," *Journal of Biomedical Optics* **15**, 021317–1–5 (2010).
- ¹²S. Mallidi, T. Larson, J. Tam, P. Joshi, A. Karpouk, K. Sokolov, and S. Emelianov, "Multiwavelength photoacoustic imaging and plasmon resonance coupling of gold nanoparticles for selective detection of cancer," *Nano Letters* **9**, 2825–2831 (2009).
- ¹³D. L. Chamberland, A. Agarwal, N. Kotov, J. B. Fowlkes, P. L. Carson, and X. Wang, "Photoacoustic tomography of joints aided by an etanercept-conjugated gold nanoparticle contrast agent: an ex vivo preliminary rat study," *Nanotechnology* **19**, 095101 (2008).
- ¹⁴J. V. Jokerst, M. Thangaraj, P. J. Kempen, R. Sinclair, and S. S. Gambhir, "Photoacoustic imaging of mesenchymal stem cells in living mice via silica-coated gold nanorods," *ACS Nano* **6**, 5920–5930 (2012), pMID: 22681633, <http://dx.doi.org/10.1021/nn302042y>.
- ¹⁵E. I. Galanzha, E. V. Shashkov, T. Kelly, J. W. Kim, L. Yang, and V. P. Zharov, "In vivo magnetic enrichment and multiplex photoacoustic detection of circulating tumour cells," *Nat Nanotechnol.* **4**, 855–860 (2009).
- ¹⁶M. E. Khosroshahi and A. Mandelis, "Combined photoacoustic ultrasound and beam deflection signal monitoring of gold nanoparticle agglomerate concentrations in tissue phantoms using a pulsed nd:yag laser," *International Journal of Thermophysics* **36**, 880–890 (2015).
- ¹⁷K. H. Song, C. Kim, C. M. Cobley, Y. Xia, and L. V. Wang, "Near-infrared gold nanocages as a new class of tracers for photoacoustic sentinel lymph node mapping on a rat model," *Nano Letters* **9**, 183–188 (2009), pMID: 19072058, <http://dx.doi.org/10.1021/nl802746w>.
- ¹⁸D. Pan, M. Pramanik, A. Senpan, S. Ghosh, S. A. Wickline, L. V. Wang, and G. M. Lanza, "Near infrared photoacoustic detection of sentinel lymph nodes with gold nanobeacons," *Biomaterials* **31**, 4088–4093 (2010).
- ¹⁹A. B. Karpouk, S. R. Aglyamov, S. Mallidi, J. Shah, W. G. Scott, J. M. Rubin, and S. Y. Emelianov, "Combined ultrasound and photoacoustic imaging to detect and stage deep vein thrombosis: phantom and ex vivo studies," *Journal of Biomedical Optics* **13**, 054061 (2008).
- ²⁰R. K. Saha and M. C. Kolios, "A simulation study on photoacoustic signals from red blood cells," *The Journal of the Acoustical Society of America* **129**, 2935–2943 (2011), <http://dx.doi.org/10.1121/1.3570946>.
- ²¹R. P. Solano, F. I. Ramirez-Perez, J. A. Castorena-Gonzalez, E. A. Anell, G. Gutierrez-Jurez, and L. Polo-Parada, "An experimental and theoretical approach to the study of the photoacoustic signal produced by cancer cells," *AIP Advances* **2**, 011102 (2012), <http://dx.doi.org/10.1063/1.3697852>.
- ²²M. W. Sigrist and F. K. Kneubhl, "Lasergenerated stress waves in liquids," *The Journal of the Acoustical Society of America* **64**, 1652–1663 (1978), <http://dx.doi.org/10.1121/1.382132>.
- ²³A. J. Dixon, S. Hu, A. L. Klibanov, and J. A. Hossack, "Oscillatory dynamics and in vivo photoacoustic imaging performance of plasmonic nanoparticle-coated microbubbles," *Small* **11**, 3066–3077 (2015).
- ²⁴A. Feis, C. Gellini, P. R. Salvi, and M. Becucci, "Photoacoustic excitation profiles of gold nanoparticles," *Photoacoustics* **2**, 47–53 (2014).
- ²⁵D. Pan, X. Cai, C. Yalaz, A. Senpan, K. Omanakuttan, S. Wickline, L. Wang, and G. Lanza, "Photoacoustic sentinel lymph node imaging with self-assembled copper neodecanoate nanoparticles," *ACS Nano* **6**, 1260–1267 (2012).
- ²⁶L. Puxiang, W. Lidai, W. T. Jian, and V. W. Lihong, "Photoacoustically guided wavefront shaping for enhanced optical focusing in scattering media," *Nat. Photon.* **9**, 126132 (2015).
- ²⁷S. Y. Emelianov, P.-C. Li, and O. M., "Photoacoustics for molecular imaging and therapy," *Phys. Today* **11**, 34–9 (2009).
- ²⁸R. Zhang, D. Pan, X. Cai, X. Yang, A. Senpan, J. S. Allen, G. M. Lanza, and L. V. Wang, " $\alpha v \beta 3$ -targeted copper nanoparticles incorporating an sn 2 lipase-labile fumagillin prodrug for photoacoustic neovascular imaging and treatment," *Theranostics* **5**, 124–133 (2015).
- ²⁹Y. Tian, H. Tian, Y. L. Wu, L. L. Zhu, L. Q. Tao, W. Zhang, Y. Shu, D. Xie, Y. Yang, Z. Y. Wei, X. H. Lu, T.-L. Ren, C.-K. Shih, and J. Zhao, "Coherent generation of photo-thermoacoustic wave from graphene sheets," *Scientific Reports* **5**, 1–8 (2015).
- ³⁰X. Chen, Y. Chen, M. Yan, and M. Qiu, "Nanosecond photothermal effects in plasmonic nanostructures," *ACS Nano* **6**, 2550–2557 (2012), pMID: 22356648, <http://dx.doi.org/10.1021/nn2050032>.
- ³¹T. Lee, Q. Li, and L. J. Guo, "Out-coupling of longitudinal photoacoustic pulses by mitigating the phase cancellation," *Scientific Reports* **6**, 1–9 (2016).
- ³²J. M. Weber, *Handbook of optical materials* (CRC Press, 2003).
- ³³C. D. Mobley, "The optical properties of water," in *Handbook of Optics: Fundamentals, techniques and design*, Vol. 1, edited by M. Bass (Optical Society of America) 2nd ed.
- ³⁴B. Reyes-Ramírez, C. García-Segundo, and A. García-Valenzuela, "An examination of polyvinylidene fluoride capacitive sensors as ultrasound transducer for imaging applications," *Measurement Science and Technology* **25**, 055109 (2014).
- ³⁵P. M. Morse and K. U. Ingard, *Theoretical Acoustics* (McGraw-Hill, New York, 1968) pp. 281–283.
- ³⁶B. Wu, C. Frez, and G. J. Diebold, "Photoacoustic transients produced by laser generated, ultrahigh thermal gradients," *Applied Physics Letters* **103**, 124105 (2013), <http://dx.doi.org/10.1063/1.4821739>.
- ³⁷H. Carslaw and J. Jaeger, *Conduction of Heat in Solids* (Oxford University Press, UK, 1959) p. 257.